Journal of Magnetic Resonance 194 (2008) 76–80

Contents lists available at ScienceDirect

Journal of Magnetic Resonance

journal homepage: www.elsevier.com/locate/jmr

Electron spin resonance spectroscopy of molecules in large precessional motion: A case of H_6^+ and $H_4D_2^+$ in solid parahydrogen

Yuta Shimizu [a], Takayuki Kumada [b,*], Jun Kumagai [a]

[a] Department of Applied Chemistry, Graduate School of Engineering, Nagoya University, Nagoya 464-8603, Japan
[b] Advanced Science Research Center, Japan Atomic Energy Agency, Tokai, Ibaraki 319-1195, Japan

ARTICLE INFO

Article history:
Received 22 April 2008
Revised 28 May 2008
Available online 3 June 2008

Keywords:
Matrix isolation
High-resolution EPR
Solid parahydrogen
H_6^+
Precession
Radiolysis

ABSTRACT

We have measured electron spin resonance (ESR) spectra of H_6^+ and $H_4D_2^+$ ions produced in γ-ray irradiated solid parahydrogen. Anisotropic hyperfine-coupling constants for H_6^+ and $H_4D_2^+$ determined by the analysis of ESR lines at 4.2 K were −0.06 and −0.12 mT, respectively, which were opposite in sign to and much smaller than theoretical results of 1.17–1.25 mT. Although no change was observed in H_6^+, the constant for $H_4D_2^+$ increased to be 1.17 mT at 1.7 K, which is very close to the theoretical value. We concluded that H_6^+ both at 4.2 and 1.7 K and $H_4D_2^+$ at 4.2 K should be in a large precessional motion with the angle of 57–59°, but the precession of $H_4D_2^+$ is stopped at 1.7 K.

1. Introduction

Study of rotational and librational motions of molecules trapped in cryocrystals has a long history [1–14]. The study was mainly carried out using infrared absorption spectroscopy (IR); however, electron spin resonance (ESR) spectroscopy is also useful [9–13]. Advantage of ESR over IR is that ESR measures pure rotational and librational motions, whereas IR induces ro-vibrational transitions.

When rotation of radicals in cryocrystals is hindered or stopped, ESR lines are broadened via anisotropic *g*-values and hyperfine interactions. On the contrary, when radicals rotate freely, such a broadening disappears due to motional narrowing [11,12]. Kumada [13] found by analysis of ESR lines of O_2 in isotopic solid hydrogens that the librational amplitude does not decrease but increases with an increase in pressure. This result indicates that cage distortion rather than size of cage is important factor which determines the librational motion [14].

In order to study the rotational and librational motions, highly resolved ESR lines are essential. Solid para-H_2 (p-H_2) is the ideal matrix for high-resolution ESR spectroscopy [15–24] for two reasons, as follows: first, p-H_2 molecules in solid p-H_2 have large zero-point vibrational motion due to their light mass and small intermolecular interactions, which repairs cracks, distortions, and imperfections, which thus keep the solid highly homogeneous without annealing [6,7,15–17]. Second, since p-H_2 has no nuclear spin moment, line broadening due to superhyperfine interaction can be avoided using purified p-H_2 matrix [16–18]. We have reported highly resolved ESR lines of H [16], CH_3 [18], C_2H_5 [17], e^- [19,20], and H_6^+ [20–23] in solid p-H_2.

H_6^+ is the radical ion, whose spectroscopic data were first reported by our group using the technique of high-resolution ESR spectroscopy with p-H_2 matrices [20–23]. We have recently carried out isotopic substitution experiments and then confirmed the assignment [23]. Fig. 1(a) shows geometry of H_6^+ calculated by Kurosaki and Takayanagi [25,26]. The H_6^+ ion has H_2^+-core on the main axis sandwiched between chemically bound two side-on H_2 groups. Isotropic hyperfine-coupling constants (HFCCs) A^{iso} experimentally determined show excellent agreement with those calculated, indicating that the calculation properly optimizes the geometry of H_6^+ (see Table 1).

Anisotropic HFCCs, A^{ani}, however, differ greatly from the theoretical ones. Recently, we carried out ESR measurements on H_6^+ and $H_4D_2^+$, both at 4.2 and 1.7 K, to conclude that the difference should be due to large precessional motion. In this paper, we present the ESR results and discuss possible precessional modes in solid p-H_2.

2. Experiment

p-H_2 (>99.5 mol %) was obtained by immersing iron hydroxide FeO(OH) into liquid normal H_2 (>99.99999%; Taiyo Nippon Sanso

* Corresponding author. Fax: +81 29 282 5939.
E-mail address: kumada.takayuki@jaea.go.jp (T. Kumada).

1090-7807/$ - see front matter © 2008 Elsevier Inc. All rights reserved.
doi:10.1016/j.jmr.2008.05.024

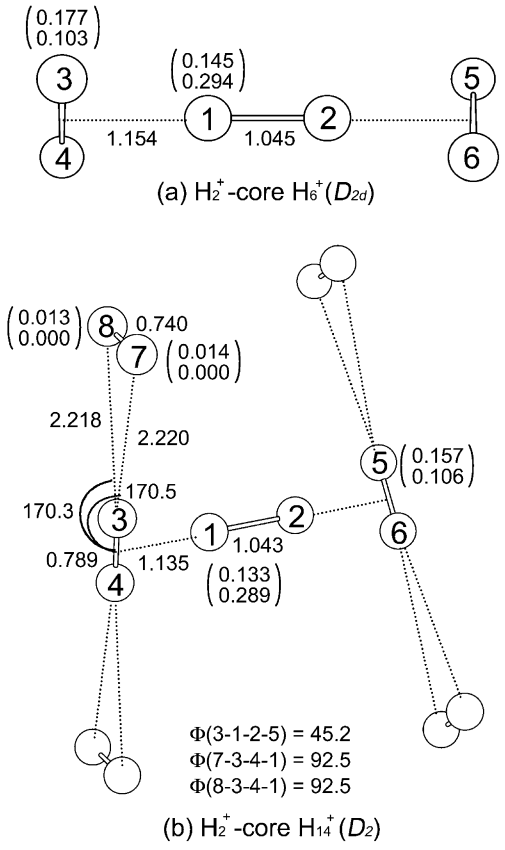

Fig. 1. Optimized geometries of H_6^+ and H_{14}^+ at the MP2/cc-pVTZ level reported by Kurosaki and Takayanagi [26]. Bond lengths in Å and angles in degrees. In parentheses are shown atomic net charge and spin density in the upper and lower lines, respectively.

Table 1
A^{iso} and A^{ani} in mT of H_6^+ and $H_4D_2^+$ in solid p-H_2 at 4.2 K experimentally determined, and of H_6^+ calculated

Level of calculation	A^{iso}		A^{ani}
	H_2^+-core	Side-on H_2 (D_2)	H_2^+-core
Experiment, H_6^+ at 4.2 K [23]	20.42	[b]	−0.06
Experiment, $H_4D_2^+$ at 4.2 K [23]	21.83, 19.43	(9.38)[a, b]	−0.12
MP2/cc-pVTZ [26]	19.690	8.745	
B3LYP/6-311++G(3df,3pd) [21]	20.079	10.263	1.17
MP2/cc-pVQZ [23]	20.231	9.007	1.25

[a] Multiplied by magnetomechanical ratio of proton to deuteron $\gamma_p/\gamma_d = 6.514$.
[b] Values for side-on H_2 in H_6^+ and $H_4D_2^+$ cannot be observed due to free rotation [23].

Co.) for 10 h at 14 K. Ortho-D_2 (o-D_2) is purified from normal D_2 (99.95%; Isotec Inc.) in the same manner at 18 K. The p-H_2 gas and p-H_2 containing o-D_2 at 1 mol % were sealed in a quartz ESR sample cell together with He (99.9999%; Taiyo Nippon Sanso Co.) at 0.1 mol %, introduced into a quartz ESR Dewar filled with liquid helium to produce solid p-H_2 at the bottom tip, and then irradiated with γ-rays for ~1 h to a total dose of 2.88 kGy at the ^{60}Co γ-ray irradiation facility at Nagoya University. The irradiated p-H_2 sample with the Dewar was used with a commercial *X*-band ESR spectrometer (JEOL JES-RE1X). Temperatures were regulated by pumping liquid helium in the quartz Dewar as measured by a Au–Fe/Chromel thermo couple (The Nilaco Co.). Microwave frequency and magnetic field were monitored by the microwave frequency counter (Hewlett-Packard, 53150A) and NMR field meter (Echo Electronics Co. Ltd., EFM-2000AX), respectively.

3. Result

Fig. 2(a) shows the quartet ESR lines (B1–B4) of H_6^+ ions in irradiated solid p-H_2. The splitting of H_6^+ lines is due to hyperfine interaction with the H_2^+-core nuclei [21–23]. The stick diagram shows resonance magnetic fields obtained by substituting the *g*-value $g = 2.002$, the isotropic HFCC for H_2^+-core $A^{iso} = 20.44$ mT, and a nuclear spin moment of H_2^+-core and its *z*-component $\{I_{12}, I_{12z}\} = \{0,0\}, \{1,-1\}, \{1,0\}$ and $\{1,1\}$ in

$$\frac{h\nu}{g\mu_B} = H_0 + A^{iso} I_{12z} + \frac{A^{iso^2}\left\{I_{12}(I_{12}+1) - I_{12z}^2\right\}}{2H_0}, \tag{1}$$

where suffixes of 1 and 2 express the positions of atoms in H_6^+ in Fig. 1(a).

The equation with these parameters completely reproduces the line positions. On the other hand, hyperfine splitting due to side-on H_2 groups was not observed, because the side-on H_2 groups near temperature 4 K are in the ground rotational state $J_{34} = J_{56} = 0$ around main axis of H_6^+, which is coupled to the $I_{34} = I_{56} = 0$ nuclear spin states.

Fig. 3 shows ESR lines of H_6^+ at $I_{12z} = \pm 1$ named B3 and B4, respectively. The asymmetric lineshape in B3 and B4 is a typical powder-pattern shape with a uniaxial asymmetric hyperfine interaction. HFCC *A* is composed of an isotropic Fermi contact term A^{iso} and anisotropic dipolar–dipolar interaction one A^{ani} [11,12],

$$A = A^{iso} + (3\cos^2\Theta - 1)A^{ani}, \tag{2}$$

for radicals having uniaxial asymmetry, where Θ is the angle with respect to magnetic field $H_0 // z$. A^{iso} determines line positions, and A^{ani} gives lineshape. The dotted lines in Fig. 3 show the simulated powder-pattern spectrum of H_6^+ with $A^{ani} = -0.06$ mT. The B3 and B4 lines measured both at 4.2 and 1.7 K are completely reproduced. The larger peaks in B3 and B4 are of H_6^+ for $\Theta = 90°$, and smaller ones are for 0°. However, as shown in Table 1, theory has predicted $A^{ani} = 1.17$–1.25 mT, positive and much larger than that experimentally determined by a factor of −20.

Fig. 2(b) shows ESR spectra of H_2^+-core $H_4D_2^+$ (C1–C16 (see Fig. 4)) produced in irradiated solid p-H_2 containing ortho-D_2 (o-D_2) at 1 mol %. Each of B1–B4 lines of H_6^+ is split into quintets in the $H_4D_2^+$ spectra due to hyperfine interaction with side-on D_2, which has $I_{56} = 0$ and 2 nuclear spin quantum numbers at $J_{56} = 0$ rotational state [23]. The stick diagram in Fig. 2(b) shows resonance fields of $H_4D_2^+$ obtained by substituting $g = 2.002$, $A_{12}^{iso} = (A_1^{iso} + A_2^{iso})/2 = 20.63$ mT, $\Delta A_{12}^{iso} = (A_1^{iso} - A_2^{iso})/2 = 1.2$ mT, isotropic HFCC of side-on D_2, $A_D^{iso} = 1.44$ mT, and *z*-component of nuclear spin quantum numbers of nuclei 1 and 2 in H_2^+-core, and side-on D_2, $I_{1z} = \pm 1/2$, $I_{2z} = \pm 1/2$, $I_{56z} = \pm 2, \pm 1, 0$ in

$$\frac{h\nu}{g\mu_B} = H_0 + A_{12}^{iso}(I_{1z}+I_{2z}) + \frac{A_{12}^{iso^2}}{2H_0}(I_{1z}-I_{2z})\sqrt{\Delta A_{12}^{iso^2} + \left(\frac{A_{12}^{iso^2}}{2H_0}\right)^2} + A_D^{iso} I_{56z}. \tag{3}$$

The line positions are completely reproduced [23]. $\Delta A_{12}^{iso} A$ is due to small difference in amplitude of zero-point motion between side-on H_2 and D_2 in $H_4D_2^+$ [28,29].

Fig. 4 shows C1–C5 and C13–C16 lines of $H_4D_2^+$ for $I_{12z} = I_{1z} + I_{2z} = \pm 1$. The C1–C5 and C13–C16 lines of $H_4D_2^+$ also look broadened by A^{ani}. The $H_4D_2^+$ lines at 4.2 K are reproduced by the simulated spectrum with $A^{ani} = -0.12$ mT, which is twice that for H_6^+, but much less than the theoretical result by a factor of −10. Unlike H_6^+, $H_4D_2^+$ was remarkably changed both in line positions and shapes by the decrease in temperature from 4.2 to 1.7 K. The C1–C5 (C13–C17) lines were shifted to upper (lower) fields by 1.2 mT. In addition, although upper (lower) peaks were more

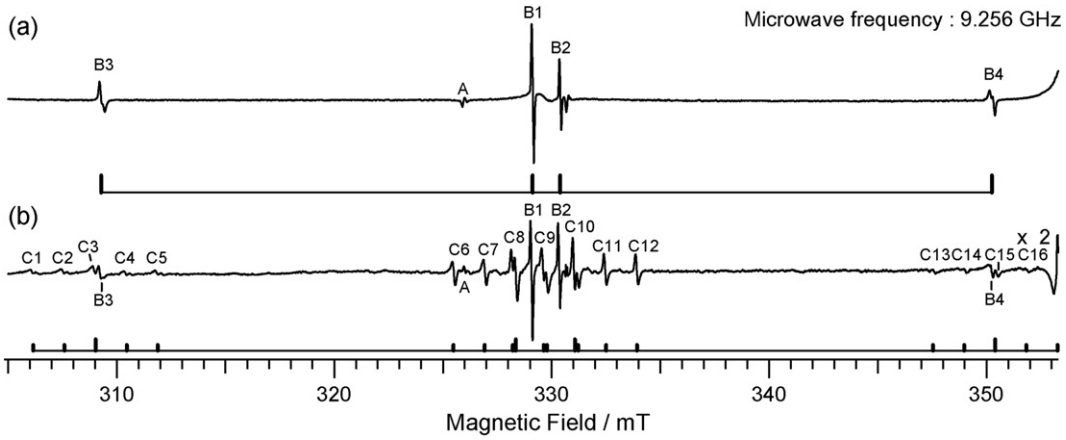

Fig. 2. ESR spectra of H_6^+ (B1–B4) and $H_4D_2^+$ (C1–C16) in γ-ray irradiated solid (a) p-H_2 and (b) p-H_2 containing o-D_2 at 1 mol % at 4.2 K with field-modulation frequency of 50 kHz, its amplitude of 0.1 mT, and microwave power of 1 mW reported by Kumagai et al. [23]. B1–B4 lines are of H_6^+, and C1–C16 ones are of H_2^+-core $H_4D_2^+$ [23]. The broad line at 330 mT is from irradiated quartz sample cell and Dewar. The line at 332 mT named A is forbidden transition of H atoms. The signals below 305 mT and above 353 mT could not be measured due to very intense H-atom lines. Note that the B1–B4 lines in (a) and (b) are saturated in intensity due to overpower and broadened due to overmodulation. The B1–B4 lines in solid p-H_2 measured with optimized microwave power and field-modulation amplitude are shown in Refs. [21,24]. Stick diagrams show resonance magnetic fields for H_6^+ in (a) and $H_4D_2^+$ in (b), respectively.

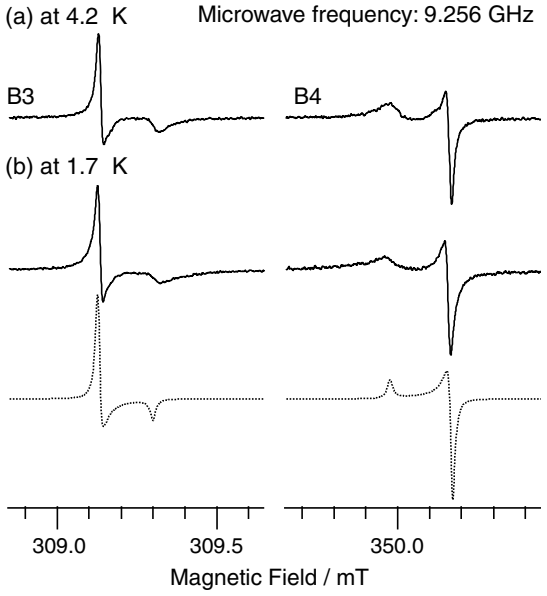

Fig. 3. ESR lines of H_6^+ at $I_{12z} = \pm 1$ (B3 and B4) in γ-ray irradiated solid p-H_2 measured with field-modulation frequency of 50 kHz, its amplitude of 0.01 mT, and microwave power of 1 mW for (a) and 0.4 mT for (b). The dashed line is a simulated spectrum of H_6^+ with $A_0^{ani} = -0.06$ mT.

intense than the lower (upper) in the C1–C5 (C13–C17) lines at 4.2 K; the lower (upper) ones became more intense at 1.7 K.

The change in lineshape of C1–C5 and C13–C17 can be explained by the change in A^{ani}. The spectrum is reproduced by the simulated one in Fig. 4(b) with $A^{ani} = 1.17$ mT, which is positive and very close to the theoretical values. The smaller peaks of C1–C5 and C13–C17 lines of $H_4D_2^+$ for $\Theta = 0°$ disappeared at 1.7 K probably due to poor signal-to-noise ratio.

Note that we have not observed any feature due to anisotropic hyperfine interaction with side-on D_2 nuclei in $H_4D_2^+$, which causes difference in lineshape and width among C1–C5 and C13–C17. Theory also predicted that the anisotropic HFCC of side-on D_2 should be much less than that of H_2^+-core by a factor of ~10 [23]. Therefore, we ignored it in the analysis of $H_4D_2^+$ lines.

4. Discussion

We propose that the discrepancy in A^{ani} between experiment and theory should be due to the local motion of H_6^+ and $H_4D_2^+$ in each cage of solid p-H_2. Although theory calculates the anisotropic HFCC A_0^{ani} against the molecular axes, ESR measures projection of A_0^{ani} on crystalline axes. Theoretical values can be compared with experimental ones only when radicals are fixed in the crystalline axes. The A^{ani} values should decrease with the increase in amplitude of precession or libration due to the motional narrowing effect.

Suppose that a radical has a precessional motion around a crystalline axis in the y-z plane with the precessional angle θ, where the unit vector r of the main axis of radical is given by

$$r(\theta,\varphi,\Theta) = \begin{pmatrix} r_x \\ r_y \\ r_z \end{pmatrix} = \begin{pmatrix} 1 & 0 & 0 \\ 0 & \cos\Theta & -\sin\Theta \\ 0 & \sin\Theta & \cos\Theta \end{pmatrix} \begin{pmatrix} \cos\varphi\sin\theta \\ \sin\varphi\sin\theta \\ \cos\theta \end{pmatrix} = \begin{pmatrix} \cos\varphi\sin\theta \\ \cos\Theta\sin\varphi\sin\theta - \sin\Theta\cos\theta \\ \sin\Theta\sin\varphi\sin\theta + \cos\Theta\cos\theta \end{pmatrix}, \tag{4}$$

with the phase of precession φ. $A^{ani}(\theta,\varphi,\Theta)$, anisotropic HFCC at Θ, θ, and phase φ, are related by

$$A^{ani}(\theta,\varphi,\Theta) = (3r_z^2 - 1)A_0^{ani}. \tag{5}$$

The expected value for $A^{ani}(\theta,\varphi,\Theta)$ in the precessional motion, is given by averaging $A^{ani}(\theta,\varphi,\Theta)$ around φ,

$$\begin{aligned} A_{pre}^{ani}(\theta,\Theta) &= \frac{\int_0^{2\pi}(3r_z^2-1)A_0^{ani}\,d\varphi}{\int_0^{2\pi}d\varphi} \\ &= \frac{3\cos^2\theta - 1}{2}(3\cos^2\Theta - 1)A_0^{ani} \\ &\equiv (3\cos^2\Theta - 1)A_{pre}^{ani}(\theta). \end{aligned} \tag{6}$$

$\theta = 0°$ corresponds to radicals completely fixed relative to crystalline axes, and $\theta = 90°$ means that each radical rotates in a plane. The anisotropy measured by ESR is $A_0^{ani}(\theta)$ related to A_0^{ani} by

$$A_{pre}^{ani}(\theta) = \frac{3\cos^2\theta - 1}{2}A_0^{ani} \tag{6'}$$

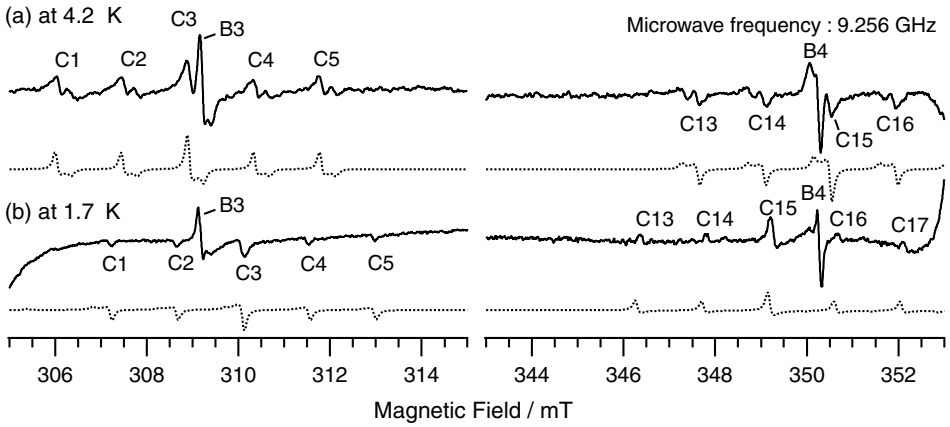

Fig. 4. ESR lines of $H_4D_2^+$ at $I_{12z} = \pm 1$ (C1–C5 and C13–C17) in γ-ray irradiated solid p-H_2 containing o-D_2 at 1 mol % with field-modulation frequency of 50 kHz, its amplitude of 0.1 mT, and microwave power of 1 mW for (a) and 0.4 mT for (b). The dashed lines are simulated spectra of $H_4D_2^+$ with $A^{ani} = -0.12$ mT for (a) and 1.17 mT for (b).

is deduced. $A_{pre}^{ani}(\theta)$, which is equal to A_0^{ani} at $\theta = 0°$, decreases with increasing θ to be $-A_0^{ani}/2$ at 90°, and crosses 0 at the magic angle of 54.74°.

On the other hand, when the radical is in librational motion with the maximum librational angle θ, the expected value, $A_{lib}^{ani}(\theta, \Theta)$, is given by,

$$A_{lib}^{ani}(\theta,\Theta) = \frac{\int_0^{\theta}\int_0^{2\pi}(3r_z^2-1)A_0^{ani}\,d\varphi\sin\theta\,d(\theta)}{\int_0^{\theta}\int_0^{2\pi}d\varphi\sin\theta\,d\vartheta} = A_0^{ani}\frac{\cos\theta(1+\cos\theta)}{2}(3\cos^2\Theta-1) \equiv A_{lib}^{ani}(\theta)(3\cos^2\Theta-1). \quad (7)$$

$A_{lib}^{ani}(\theta)$, corresponding to A_0^{ani} at $\theta = 0°$, decreases with an increase in θ to be 0 at 90°, which corresponds to free rotational state. Unlike $A_{pre}^{ani}(\theta)$, the sign of $A_{lib}^{ani}(\theta)$ cannot be negative for $0° \leqslant \theta \leqslant 90°$ and $A_0^{ani} > 0$. Therefore, a negative value of A^{ani} in H_6^+ at 4.2 and 1.7 K, and $H_4D_2^+$ at 4.2 K should be due to a large precessional motion with $\theta > 54.74°$, but not due to libration!

We determined θ in Table 2 by substituting the experimental value of A^{ani} to $A_{pre}^{ani}(\theta)$, and the theoretical one to A_0^{ani} in Eq. (6), respectively. $\theta = 57°$ is obtained for H_6^+ at 4.2 and 1.7 K, and 59° for $H_4D_2^+$ at 4.2 K, but only 12° for $H_4D_2^+$ at 1.7 K.

Let us consider possible precessional mode of H_6^+ and $H_4D_2^+$ in solid p-H_2. Fig. 1(b) shows the optimized geometry of H_{14}^+ [26]. Since H_{14}^+ is composed of H_6^+ and physically bound outer four H_2s we can use the outer H_2s to resemble H_2 molecules around H_6^+ in solid p-H_2. The equilibrium H_6^+—H_2 distance is 3.2 Å, which is close to the intermolecular distance of solid p-H_2 (3.793 Å [27]). Therefore, H_6^+ should be trapped in a single substitutional cage of solid p-H_2.

Fig. 5 shows a model of H_6^+ trapped in a single substitutional hcp cage of solid p-H_2. The cage has 8 trianglar and 6 square planes.

Table 2
A^{ani} and θ of H_6^+ and $H_4D_2^+$ in solid p-H_2

	Temperature/K	A^{ani}/mT	θ[b]/degree
H_6^+	4.2	−0.06	57
	1.7	−0.06	57
$H_4D_2^+$	4.2	−0.12	59
	1.7	1.17	12
Theory[a]		1.25	

[a] Theoretical value is obtained at the MP2/cc-pVQZ level of calculation.
[b] Precession angle θ obtained by substituting experimental value in A_{pre}^{ani}, and theoretical one in A_0^{ani} of Eq. (6) (see text).

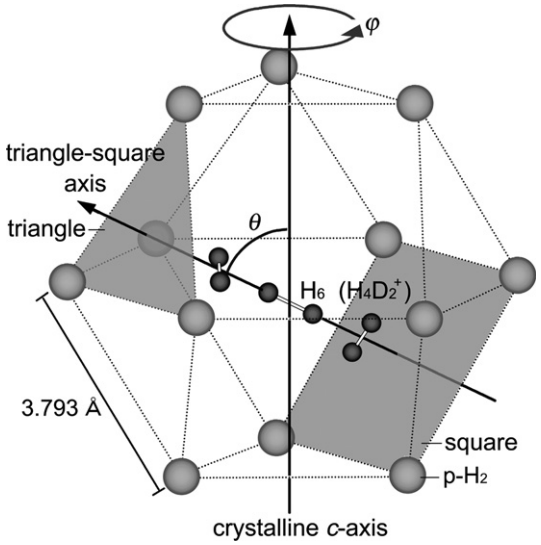

Fig. 5. Schematic representation of H_6^+ trapped in a single substitutional hcp cage of solid p-H_2.

All trianglar planes at the side diagonally face to the square ones, but the trianglar plane at the top faces to the trianglar one at the bottom. We propose that the main axis of H_6^+ should be along the axis passing through centers of a pair of diagonally faced square and triangle planes (triangle–square axis) in order to avoid overlap of electronic orbital between H_6^+ and p-H_2s. When H_6^+ in the axis is off-centered from the center of cages to the square by 0.3 Å, the distances between side-on H_2 of H_6^+ to each p-H_2 molecule at the apexes of triangle and square are calculated to be 2.8 Å. This value is very close to the distance between a side-on H_2 of H_6^+ and an outer H_2 in Fig. 1(b) of 2.6 Å. Eventually, these values should be larger than 2.6 Å when the effect of nuclear quantum fluctuation is taken into account on the calculation [28,29]. This result indicates that H_6^+ should be trapped along the triangle–square axis with little distortion of the hcp cage of solid p-H_2.

On the other hand, when H_6^+ is aligned along the *c*-axis of solid p-H_2, the distance between side-on H_2 and p-H_2 molecules at the apexes of upper and lower triangles is 2.6 Å, being a little shorter than the equilibrium distance expected when taking into account the nuclear quantum fluctuation. Therefore, H_6^+ should prefer the triangle–square axes rather than *c*-axis.

We suggest that the H_6^+ ions are in precessional motion along *c*-axis by jumping among the six equivalent triangle–square axes

in solid p-H_2. When the cage is not distorted, the angle between *c*-axis and triangle–square axis in the hcp cage is calculated to be $\theta_{min} = 63.2°$, which is very close to the precessional angle of H_6^+ at 4.2 and 1.7 K (57°), and $H_4D_2^+$ at 4.2 K (59°) determined experimentally.

The similar values of A^{ani} between experiment and theory in $H_4D_2^+$ at 1.7 K indicate that the precessional motion is stopped. Why is the precessional motion stopped in $H_4D_2^+$ but not in H_6^+? We propose two possible reasons as follows: first, the moment of inertia for $H_4D_2^+$ is larger than that for H_6^+. $H_4D_2^+$ is heavier than H_6^+, and, unlike H_6^+, the center of mass does not coincide with the center of geometry in $H_4D_2^+$. Second, not only the nuclear configuration but also the electronic wave function of $H_4D_2^+$ no longer has D_{2d} symmetry but has C_{2v} [23]. This means that the energy $E(\theta_{min}, \varphi)$ of $H_4D_2^+$ in the hcp cage of solid p-H_2 does not have 6-fold but has 3-fold symmetry around φ. $H_4D_2^+$ should be localized in one of three deeper potential wells at 1.7 K.

We have no idea whether the precession of H_6^+ is due to quantum mechanical tunneling or classical thermal hopping. Small mass and matching in energy levels between neighboring wells are essential for quantum tunneling. Because of the small moment of inertia and high symmetry, H_6^+ may keep the precession via the tunneling down to 0 K. On the other hand, the rate for the tunneling precession should be much less in $H_4D_2^+$, because of larger moment of inertia and lower symmetry in potential for precession.

In conclusion, we have compared anisotropic HFCC of H_6^+ and $H_4D_2^+$ in solid p-H_2 determined by the analysis of ESR lines with theoretical calculation to find the results as follows: H_6^+ is in precessional motion at precessional angle of 57° along the *c*-axis of substitutional hcp cage in solid p-H_2 both at 4.2 and 1.7 K. Although $H_4D_2^+$ is also in the precessional motion at 4.2 K, the precession is stopped at 1.7 K. The difference should be due to larger moment of inertia and lower molecular symmetry in $H_4D_2^+$.

Local environment of cages around guest molecules and their local motions should be determined in order to study solid-phase chemical reaction between guest and host molecules. Recently, we have observed the reactions related to H_6^+ such as $H_6^+ + H_2 \rightarrow H_2 + H_6^+$ and $H_6^+ + e^- \rightarrow 3H_2$ in solid p-H_2. We hope that the mechanism of solid-phase reactions related to H_6^+ can be clarified through this study.

Acknowledgments

The authors are grateful to Dr. Yuzuru Kurosaki in the Japan Atomic Energy Agency, Professor Toshiyuki Takayanagi in Saitama University, and Professor Anders Lund in Linköping University for discussion.

References

[1] V.A. Apkarian, N. Schwentner, Molecular photodynamics in rare gas solids, Chem. Rev. 99 (1999) 1481–1514.
[2] V.E. Bondybey, A.M. Smith, J. Agreiter, New developments in matrix isolation spectroscopy, Chem. Rev. 96 (1996) 2113–2134.
[3] G. Schallmoser, A. Thoma, B.E. Wurfel, V.E. Bondybey, Rotation of CN in solid rare gases, Chem. Phys. Lett. 219 (1994) 101–106;
B.E. Wurfel, N. Caspary, J. Agreiter, A. Thoma, A.M. Smith, V.E. Bondybey, Medium effects on weakly-bound complexes—Xe–CN in solid rare-gases, J. Chim. Phys. 92 (1995) 351–361.
[4] W.H. Flygare, Molecular rotation in the solid state. Theory of rotation of trapped molecules in rare-gas lattices, J. Chem. Phys. 39 (1963) 2263–2273.
[5] H. Friedmann, S. Kimel, Theory of shifts of vibration–rotation lines of diatomic molecules in noble-gas matrices. Intermolecular forces in crystals, J. Chem. Phys. 43 (1965) 3925–3939.
[6] T. Oka, High-resolution spectroscopy of solid hydrogen, Ann. Rev. Phys. Chem. 44 (1993) 299–333.
[7] S. Tam, M.E. Fajardo, H. Katsuki, H. Hoshina, T. Wakabayashi, T. Momose, High resolution infrared absorption spectra of methane molecules isolated in solid parahydrogen matrices, J. Chem. Phys. 111 (1999) 4191–4198.
[8] H. Hoshina, T. Wakabayashi, T. Momose, T. Shida, Infrared spectroscopic study of rovibrational states of perdeuterated methane (CD_4) trapped in parahydrogen crystal, J. Chem. Phys. 110 (1999) 5728–5733.
[9] T. Yamada, K. Komaguchi, M. Shiotani, N.P. Benetis, A.R. Sorners, High-resolution EPR and quantum effects on CH_3, CH_2D, CHD_2, and CD_3 radicals under argon matrix isolation conditions, J. Phys. Chem. A 103 (1999) 4823–4829.
[10] K. Komaguchi, T. Kumada, T. Takayanagi, Y. Aratono, M. Shiotani, T. Miyazaki, H atom–H_2 molecule van der Waals complexes in solid argon matrix by high-resolution ESR spectroscopy, Chem. Phys. Lett. 300 (1999) 257–261.
[11] C.P. Poole Jr., Electron Spin Resonance, second ed., Dover, Mineola, 1983.
[12] A. Abragam, The Principle of Nuclear Magnetism, Oxford University Press, Oxford, 1961.
[13] T. Kumada, Rotation of O_2 molecules in solid D_2 and HD: an electron spin resonance study, J. Chem. Phys. 117 (2002) 10133–10138.
[14] Z. Li, V.A. Apkarian, Impurity rotations in quantum versus classical solids: O_2 in solid hydrogens, J. Chem. Phys. 107 (1997) 1544–1550.
[15] T. Kumada, N. Kitagawa, T. Noda, J. Kumagai, Y. Aratono, T. Miyazaki, An ENDOR spectrum of H atoms in solid H_2, Chem. Phys. Lett. 288 (1998) 755–759.
[16] T. Kumada, M. Sakakibara, T. Nagasaka, H. Fukuta, J. Kumagai, T. Miyazaki, Absence of recombination of neighboring H atoms in highly purified solid parahydrogen: electron spin resonance, electron–nuclear double resonance, and electron spin echo studies, J. Chem. Phys. 116 (2002) 1109–1119.
[17] T. Kumada, J. Kumagai, T. Miyazaki, High-resolution electron spin resonance spectroscopy of ethyl radicals in solid parahydrogen, J. Chem. Phys. 114 (2001) 10024–10030.
[18] T. Miyazaki, K. Yamamoto, J. Arai, Effect of rotational quantum states (J = 0, 1) of matrix H_2 molecules on ESR spectra of radicals at 4.2 K, Chem. Phys. Lett. 219 (1994) 405–408.
[19] T. Kumada, N. Kitagawa, S. Mori, J. Kumagai, Y. Aratono, T. Miyazaki, Observation of electron bubbles in para-H_2–D_2 (HD) mixtures by high-resolution esr spectroscopy, J. Phys. Chem. A 103 (1999) 8966–8968.
[20] T. Kumada, Y. Shimizu, T. Ushida, J. Kumagai, H_6^+, H_5D^+, $H_4D_2^+$, and $H_2D_4^+$ produced in γ-ray irradiated solid para-H_2, Radiant. Phys. Chem., in press.
[21] T. Kumada, H. Tachikawa, T. Takayanagi, H_6^+ in irradiated solid *para*-hydrogen and its decay dynamics: reinvestigation of quartet electron paramagnetic resonance lines assign H_2^-, Phys. Chem. Chem. Phys. 7 (2005) 776–784.
[22] T. Kumada, T. Takayanagi, J. Kumagai, ESR study of H_6^+ and $H_4D_2^+$ produced in irradiated solid hydrogens, J. Mol. Struct. 786 (2006) 130–133.
[23] J. Kumagai, H. Inagaki, S. Kariya, T. Ushida, Y. Shimizu, T. Kumada, Electron spin resonance study on H_6^+, H_5D^+, $H_4D_2^+$, and $H_2D_4^+$ in solid parahydrogen, J. Chem. Phys. 127 (2007) 024505.
[24] J. Kumagai, M. Hanabusa, H. Inagaki, S. Kariya, Is the ESR spectrum attributable to H_2^- or $H_2^+(H_2)_2$? Precise measurement of the *g*-value and anisotropic hyperfine structure in γ-irradiated solid parahydrogen, Phys. Chem. Chem. Phys. 6 (2004) 4363–4368.
[25] Y. Kurosaki, T. Takayanagi, A direct isomerization path for the H_6^+ cluster: an ab initio molecular orbital study, Chem. Phys. Lett. 293 (1998) 59–64.
[26] Y. Kurosaki, T. Takayanagi, An ab initiomolecular orbital study of even-membered hydrogen cluster cations: H_6^+, H_8^+, H_{10}^+, H_{12}^+, and H_{14}^+, J. Chem. Phys. 109 (1998) 4327–4334.
[27] I.F. Silvera, The solid molecular hydrogens in the condensed phase: fundamentals and static properties, Rev. Mod. Phys. 52 (1980) 393–452.
[28] A. Kakizaki, T. Takayanagi, M. Shiga, A direct isomerization path for the H_6^+ cluster: an ab initio molecular orbital study, Chem. Phys. Lett. 449 (2007) 28–32.
[29] Y. Kurosaki, Y. Shimizu, J. Kumagai, Isotope effects on the spin-density distribution in the H_6^+ clusters: direct ab initio molecular dynamics study, Chem. Phys. Lett. 455 (2008) 59–63.